Scilight

Environmental Pollution, Risk, and Remediation Insights

https://www.sciltp.com/journals/eprri

Article

Nano-Alumina Functionalized Carbon Composite Adsorbent from Coir Pith Biomass for Fluoride Removal from Aqueous Solution

Shanmugasundaram Prema Suriyaraj [1,2,3] and Rajendran Selvakumar [1,*]

[1] Nanobiotechnology Laboratory, PSG Institute of Advanced Studies, Peelamedu, Coimbatore 641004, India
[2] School of Applied Bioscience, Food and Agri Tech, Rathinam Global Deemed to be University, Eachanari, Coimbatore 641021, India
[3] Rathinam Technical Campus, Eachanari, Coimbatore 641021, India
* Correspondence: rsk@psgias.ac.in; Tel.: +91-422-4344328

How To Cite: Suriyaraj, S.P.; Selvakumar, R. Nano-Alumina Functionalized Carbon Composite Adsorbent from Coir Pith Biomass for Fluoride Removal from Aqueous Solution. *Environmental Pollution, Risk, and Remediation Insights* **2026**, *1*(1), 6. https://doi.org/10.53941/eprri.2026.100006

Received: 22 January 2026
Revised: 4 July 2026
Accepted: 25 August 2026
Published: 24 September 2026

Abstract: Fluoride contamination in surface and groundwater was a major environmental issue in various parts of the world. Fluorosis is caused by consumption of contaminated water; hence, it is essential to treat fluoride from contaminated water sources. This study involves the development of nano-alumina functionalized carbon composite adsorbent (NAAC) nanocomposite under controlled atmosphere for adsorption of fluoride from water. NAAC was synthesized using carbonization process at controlled nitrogen atmosphere. The X-ray diffraction (XRD), (High Resolution Transmission Electron Microscopy) HR-TEM coupled with (Energy Dispersive X-ray Spectroscopy) EDS and (Selected Area Electron Diffraction) SAED were used for characterization of the NAAC. Adsorption capacity of NAAC of fluoride was evaluated by batch and column mode using the fluoride spiked solution. The experiments performed to identify initial concentration of adsorbate and desorption studies. Adsorption data fitted to relevant Isotherm & Kinetic models. (Q_0) of NAAC was found as 58.82 mg/g. Effects of flow rate, bed volume and different F- concentrations for the column experiments were find. (Bed-Depth-Service-Time) BDST model achieved by using data collected from experiments. As a result, the batch sorption was found to be more effective than the column sorption for removal. Therefore, study done the production of low-cost adsorbent fluoride removal from groundwater made by using NAAC is possible.

Keywords: nano-alumina; activated carbon; nanocomposite; fluoride; batch; column mode

1. Introduction

Pollution at groundwater has key concern in major parts of World [1]. India is one of the 23 countries in the World, which is facing fluoride contamination in groundwater causing several health issues. Fluoride pollution is common in “Gujarat; Rajasthan; Uttar Pradesh; Tamil Nadu; Andra Pradesh; and West Bengal” of India [2,3]. High amount of fluoride intake may lead to demineralization of tooth causing cavities, alzheimer syndrome, bladder cancer, Thyroid problem, gastrointestinal bleed and Osteosclerosis [4]. Unfortunately, there is no clinical treatment available for Fluorosis, the fluoride related health hazards. Bureau of Indian Standard (BIS) has prescribed 1.5 mg/L fluoride concentration at drinking water, beyond which these fluorides induced disease manifestations persist [5]. Scientific studies have shown that adsorption is the most proficient; cost-effective

method for fluoride remove from water rather than any other alternative methods [6,7]. Adsorbents like activated alumina, carbon, mixed metal oxides, bio-adsorbents, natural wastes, miscellaneous adsorbents and recent nano-adsorbents have been extensively studied for their fluoride removal capacity. There are numerous advanced nanomaterials reported in the recent years, but there is a scope of discovering new materials with enhanced fluoride adsorption capacity and cost effective. Development of sustainable defluoridation techniques using materials with safe removal for fluoride from groundwater is the need of the hour [8]. Carbonization and Activation of different natural wastes showing good percentage of defluoridation, could be considered as novel approach in Adsorbents preparation process [9]. There are various reports for the use of activated carbon for fluoride adsorption in a low cost. The surface of activated carbon produced from bio sources can be tailored to improve the F- adsorption. The activated carbon has been functionalized with various metal nanoparticles like Fe_3O_4 [10], aluminium nanoparticle [11], Cadmium selenide nanoparticles [12], Ce-Al oxide nanoparticle [13], nanostructured magnesia [14], cerium [15] etc., for enhancing its fluoride removal property. Despite of these functionalization process, the need for even distribution of nanomaterials, high surface area carbon, pH optimization, industrial scalability, low loading capacity, less regeneration cycle efficiency, and high production cost have been key challenges faced for effective adsorbent synthesis using nanomaterials have been the challenges faced for use of nanoparticle functionalized activated carbon [11,16]. Hence in this paper, we have investigated the functionalization of nanoparticles on coir pith biomass based activated carbon surface under controlled condition to address these issues and investigated its fluoride adsorption property in both batch and column mode experiments. This material was effective for fluoride removal from water and cost-effective. Various materials such as metal-organic frameworks and hybrid carbon composites are used for removal of fluoride from water by researchers. These materials are really good at picking up fluoride. Can be used again and again. Some people have already used nano-alumina and carbon to remove fluoride. This study is different. This study is about making a kind of carbon from coir pith and adding nano-alumina to it in a very controlled way. This makes the carbon work better. Is also good for the environment. The way we made this material is new and can be used to make a lot of it. We tested this material in two ways, which helps us understand if it can be used in real life to remove fluoride from water. The metal-organic frameworks and hybrid carbon composites are still important. This study is focused on the coir pith-derived carbon matrix, with nano-alumina.

2. Materials and Methods

2.1. Materials

$Al(OH)_3$ (Aluminum hydroxide) (purity > 99.9%, Sigma-Aldrich, Karnataka, India) was used as a precursor of aluminum. The coir pith was collected from the local agricultural waste of Coimbatore district, India. A Standard fluoride solution (1000 ppm) and 1,2-cyclohexanediaminetetraacetic (Total Ionic Strength Adjustment Buffer Solution) TISAB were procured with Thermo Scientific, Waltham, MA, USA. Purified water used for the preparation of solutions using a Millipore system with a resistivity of (18.2 MΩ·cm at 25 °C).

2.2. Synthesis of Nano-Alumina Functionalized Carbon Composite Adsorbent (NAAC)

The nano-alumina functionalized carbon composite adsorbent (NAAC) was prepared by washing the coir pith for several times to remove adhered soil particles, dust, soluble impurities and other surface contaminants with running tap water, to get rid of the dissolved salts & impurities left over it was again washed three times using distilled water. The washed biomass was dried in air at room temperature (28 ± 2 °C) for 48 h until a constant weight was obtained prior to further processing. A 5% (*w*/*v*) aqueous suspension of aluminum hydroxide [$Al(OH)_3$] was prepared by dispersing 5 g of $Al(OH)_3$ powder in 100 mL of ultrapure Millipore water under continuous magnetic stirring. The suspension thus obtained directly used for the impregnation of the coir pith. To the freshly prepared suspension, 10 g dried coir pith was added and stirred for 15 min for uniform coating of aluminum hydroxide particles on the surface of biomass. The mixture air-dried at room temperature for two consecutive days to remove moisture prior to carbonization. A unique indigenous reactor setup was developed for maintaining partial oxygen condition for effective carbonization of coirpith biomass and used for the study (Figure 1). The aluminum hydroxide treated coirpith biomass was filled tightly in inner vessel to maximum occupancy and pressed maximum to avoid air gap and sealed using tight lid. The inner vessel was placed in a larger vessel layered with fine sand sieved using 0.35 mm sieve at the bottom. Further the sides were also filled with same 0.35 mm fine sand to cover the inner vessel completely to the brim. The vessel gap was purged with nitrogen to replace oxygen in the sand pore. The sealed reactor was heat at 700 °C for 1 h under ambient air using a muffle furnace. The sealed reactor kept the conditions oxygen-limited by the nitrogen purging that preceded, not by nitrogen supplied to the

furnace chamber. After carbonization, the vessel was cooled to room temperature then the carbonized biomass was recovered, powdered using mortar and pestle, sieved (0.35 mm) and used for further studies.

The synthesis repeated in three independent batches under the same conditions to confirm the reproducibility of the material properties. Small differences in yield and particle size distribution were within acceptable experimental variation.

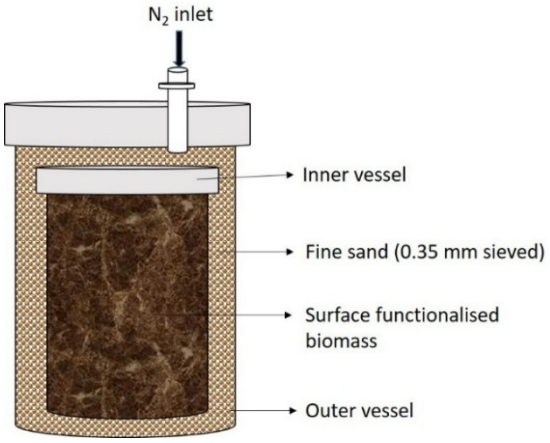

Figure 1. Schematic diagram of indigenous reactor used for NAAC preparation.

2.3. Characterization

The NAAC was studied based on the method described by [17]. XRD analysis was performed using an X-ray diffractometer to determine the phase and crystal structure of the NAAC. The diffractometer used CuKα radiation with a wavelength of 1.5400 Å. The settings were 30 mA, 40 kV, a step size of 0.05 (2θ), and a scan step time of 10.16 s in continuous scan mode. For the High-Resolution Transmission Electron Microscopy (HR-TEM) analysis, about 1 mg of NAAC was mixed with 10 mL of ultra-pure milli-Q water (18.2 MΩ·cm) and sonicated for 15 min. The resulting mixture was placed on a 300-mesh carbon-coated copper grid and left to stand at room temperature. Morphological features were examined using a HR-TEM (JEOL JEM-2100, Tokyo, Japan) at an acceleration voltage of 200 kV. The elemental composition of the adsorbent was analyzed using an EDS detector attached to the HR-TEM.A drop of the suspension was placed on a carbon-coated copper grid (300 mesh) and left at room temperature before being analyzed using the HR-TEM at 200 kV. The chemical composition of the adsorbent was examined using Energy Dispersive X-ray Spectroscopy (EDS) in conjunction with the HR-TEM images.

Physicochemical properties of NAAC, such as yield (%), pH, decolorizing capacity, apparent density, specific gravity, and porosity (%) were analyzed based on the standardized protocols. Yield (%) was determined through the calculation of the ratio between the mass of carbonized NAAC after synthesis and the initial dry mass of the biomaterials. pH value of NAAC adsorbent is determined in 1:10 (w/v) mixture of adsorbent with water using digital pH meter after incubation for 30 min. The apparent density was determined by measuring the mass of NAAC adsorbent that occupied a certain volume in the graduated cylinder without compaction. Specific gravity was analyzed by the pycnometer method. Porosity (%) was calculated using the equation which involved the values of apparent density and particle density. Decolorizing capacity was determined according to the standard protocol for methylene blue adsorption.

2.4. Estimation of Fluoride

The concentrations of fluoride measured by Orion Four-Star ion-selective electrode (Thermo Fisher Scientific, Waltham, MA, USA) as per the guidelines set by ASTM D1179. Calibration of the ion-selective electrode for the fluoride analysis done according to ASTM D1179. Before the measurement, the equal volumes of TISAB solution with CDTA is add to the standards and samples. 0.1 mg L^{-1} is the detection limit of this method.

2.5. Batch Adsorption Studies

Synthesized material were used like adsorbent material in aqueous solution by batch adsorption method to remove fluoride. The determination of effective removal of fluoride was studied by determining the impact of contact time and initial fluoride concentration. To find the best contact time for maximum fluoride adsorption from the solution, different fluoride concentrations (ranging from 2 to 10 mg/L) were used. Each test involved placing 0.2 g of the adsorbent material in plastic flasks with 200 mL of the solution. Then solution kept at neutral pH at

room temperature. Samples of 2 mL taken out at certain intervals with a micropipette, filtered by 0.45 μm filter, and checked for residual fluoride ions. The amount of sample fluid taken was less than 5% of the total volume of the reaction, 50 mL, so the ratio of solid to liquid and pH of the solution remained unchanged throughout the whole absorption. Control tests were done without using any adsorbent to check how much fluoride is absorbed by the flasks. Adsorption percentage was calculated according to Equation (1). solution was kept at a neutral pH and at room temperature. At specific times, 2 mL samples were taken using a micropipette and then filtered through a 0.45 micrometer filter to measure the remaining fluoride ions. Because the amount of sample taken was less than 5% of the total 50 mL reaction mixture, there was almost no change in the solid-liquid ratio or pH during the experiment. Control tests were done without any adsorbent to check if the flasks themselves adsorbed fluoride. The percentage of fluoride removed was calculated using Equation (1).

$$\text{Percentage F- removal} = (C_i - C_f)/C_i \times 100 \quad (1)$$

C_i is the starting amount of fluoride in the solution, and C_f is the amount left after the process. To study how fast the adsorption happens, 0.5 g of NAAC was used with 50 mL of fluoride solution that had a known starting concentration. The mixture was stirred at 150 revolutions per minute and kept at room temperature, which is around 28 degrees Celsius, plus or minus 2 degrees. At set times, samples were taken and tested to find out how much fluoride was left until the process reached balance. The fluoride concentration was measured using a special electrode that detects fluoride ions. Equilibrium contact time obtained from the kinetics study (240 min) was used for all adsorption isotherm experiments. Inu adsorption isotherm studies, fluoride solutions of different initial concentrations (e.g., 2–20 mg L^{-1} or actual initial concentration), were subjected to 0.5 g NAAC/50 mL at the optimum pH under the same agitation time until equilibrium contact time. The suspensions were then filtered and equilibrium concentration of fluoride (C_e) was determined. The q_e was calculated, and the data were fitted to the Langmuir and Freundlich adsorption isotherms. The kinetics data were analyzed using the pseudo-first order, pseudo-second order, and intraparticle diffusion kinetics models. Batch adsorption tests were performed in duplicate. The q_e was calculated, and the data were fitted to the Langmuir and Freundlich adsorption isotherms. The kinetics data were analyzed using the pseudo-first, second order, and intraparticle diffusion kinetics models. Batch adsorption tests were performed in duplicate.

2.6. Column Mode Adsorption Studies

The adsorption ability of NAAC towards fluoride ions was evaluated in the column mode. The plastic column was charged with 35.32 cm^3 bed volume of the nanocomposite (50 × 2.5 cm^2). After adjusting the solution's pH to the best level, the solution with 6 mg/L of fluoride was run through the column at different speeds: 2.5, 5, 7.5, and 10 mL per minute. The liquid that came out was collected at regular times, and the fluoride levels in each part were checked. The most effective amount of resin was found by testing columns with bed volumes of 17.66, 35.32, 52.98, and 70.65 cm^3. The experiment was done again using the most appropriate flow rate and bed volume. For each experiment, the F- conc in selected range 2.0–10.0 mg/L were used. The fluoride ion removal capacity by the flow volume can be calculated as C_t/C_o, which represents the ratio of the amount of F- adsorbed to the amount of F- introduced into the column. C_o and C_t are conc of adsorbate at inlet & outlet of column. The total amount of sorbate removed in the column for a particular feed concentration is equivalent to area under curve of plot of C_t versus eluant volume. The data obtained were plotted as BDST curves.

2.7. Desorption Studies

The NAAC used in batch adsorption experiment uptake 10 mg/L of F- were separated and rinsed three times with ultrapure Millipore water (18.2 MΩ cm). The same procedure was repeated for other samples. The used adsorbent was combined with 100 mL of distilled water that had various levels of NaOH (from 0% to 10%) and stirred for a set period until it reached equilibrium. The amount of fluoride ions removed was then measured as described earlier. Every test was done three times to ensure accuracy. The used adsorbent was combined with 100 mL of distilled water that had various levels of NaOH (from 0% to 10%) and stirred for a set period until it reached equilibrium. The amount of fluoride ions removed was then measured as described earlier. Every test was done three times to ensure accuracy.

3. Results and Discussion

The synthetic NAAC showed low solubility in aqueous solution and solid-phase stability during the entire process of adsorption. Leaching of alumina nanoparticles was not detected, proving the applicability of NAAC for both batch and column studies. Characterization of NAAC was carried out to understand its surface morphology and its crystal structure properties. XRD pattern of NAAC are shown in Figure 2. XRD pattern for NAAC shows the appearance of a broad halo in the 2θ region of 20–30°, which suggests that the activated carbon matrix is

amorphous. Further, there are diffraction peaks at 2θ = 24.3°, 33.2°, 41.0°, and 49.5° (needs update with actual position of diffraction peaks), which correspond to (012), (104), (113), and (116) crystal planes, respectively, having interplanar d-spacings of 3.66 Å, 2.69 Å, 2.20 Å, and 1.84 Å, respectively (needs update with d-values). The diffraction peaks are assigned to the crystallographically well-defined rhombohedral phase of alumina having parameter a = b = 4.760 Å and c = 12.993 Å belonging to space group R3c, No. 167, which matches with the data available in JCPDS card No. 81-1667. The occurrence of alumina diffraction peaks along with the broad amorphous carbon background indicates that the alumina has been successfully integrated into the activated carbon matrix.

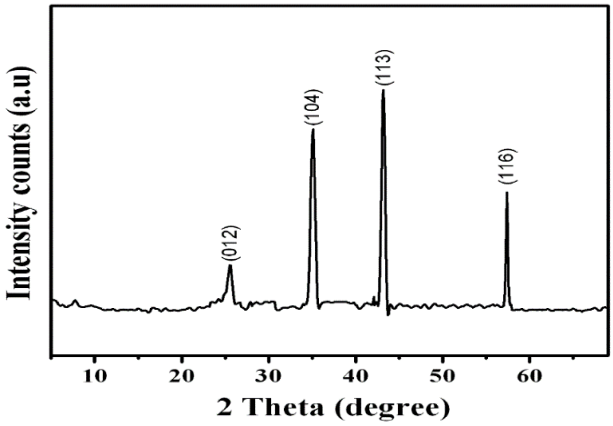

Figure 2. X-ray diffraction pattern of NAAC.

HR-TEM images from prepared NAAC displayed in Figure 3A. Image shows that spherical alumina nanoparticles were uniformly distributed in the activated carbon. The SAED pattern of the synthesized NAAC nanoadsorbent was in agreement with corresponding XRD results (Figure 3A insert). The high resolution image of the NAAC is shown in the Figure 3B. The crystalline nature of the alumina nanoparticle and the amorphous carbon was clearly differentiated in the high resolution image. The size of the nano-alumina in the activated carbon was found to be 16 ± 5.2 nm (Figure 3C). EDS spectrum illustrates existence of Al, O & C elements in NAAC (Figure 3D). properties of NAAC were given in Table 1.

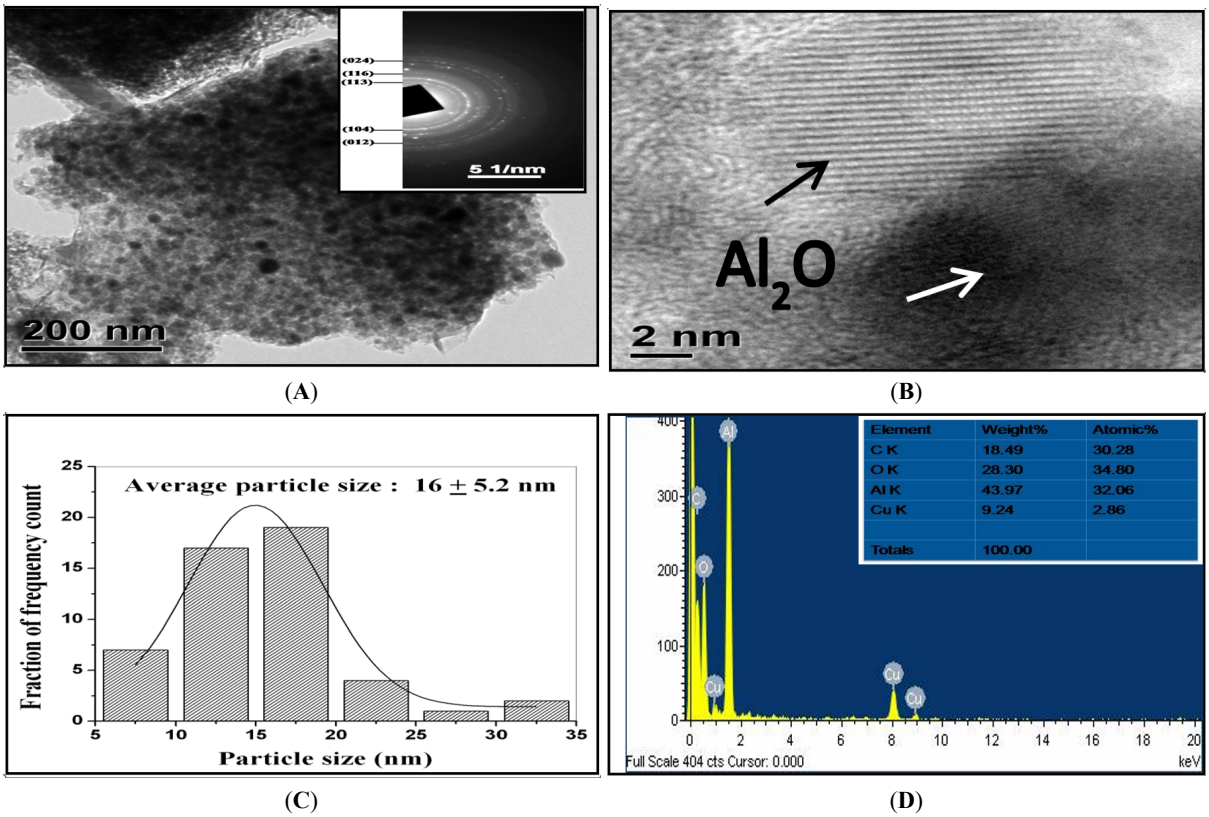

Figure 3. HR-TEM image for NAAC (**A**), SAED pattern of the corresponding image (A-insert), high resolution image (**B**), particle size distribution (**C**), EDS of NAAC (**D**) nanocomposite.

Table 1. Properties of the synthesized NAAC.

Properties	NAAC
Yield (%)	56.7 ± 0.02
pH	7.3 ± 0.13
Decolorizing power (mg/g)	30 ± 0.24
Apparent density (g/mL)	0.8 ± 0.31
Specific gravity (W_a/v)	2.9 ± 0.07
Porosity (%)	53 ± 0.72

3.1. Fluoride Adsorption Using NAAC by Batch Process

3.1.1. Effect on Contact Time & Initial Concentration on F- Adsorption

The use of NAAC helped remove fluoride effectively, as shown by the increase in removal percentage with longer contact time, and it stayed the same once equilibrium was reached (Figure 4). It took 50 min to reach equilibrium when the initial fluoride concentration was 2 mg/L, and 60 min when it was 4, 6, 8, or 10 mg/L. The removal percentage for 2 mg/L fluoride was 92%, but it dropped from 92% to 54% as the initial fluoride concentration increased to 10 mg/L. The removal percentage versus time curves were smooth and continuous, pointing to a single layer of fluoride on the outer surface of the adsorbent [6]. Even though the percentage of fluoride adsorbed decreased with higher initial concentration, the amount adsorbed per gram of adsorbent increased. From the data in Figure 4, it was seen that the amount of adsorbate increased with reaction time and remained constant after reaching equilibrium. This change in removal percentage could be because there were initially more empty spots on the adsorbent surface and a strong concentration gradient. Later, the uptake of fluoride dropped quickly after a certain contact time due to fewer adsorption sites becoming available. Ref. [18] studied manganese-oxide-coated alumina and found that most fluoride sorption happened within 3 h of contact time. After that, the rate of adsorption became very slow, and the fluoride concentration in the solution stayed almost the same. Ref. [19] reported that rapid fluoride adsorption occurred with sulfate-doped Fe3O4/Al2O3, followed by a slower adsorption process. About 90% of fluoride was removed in 20 min, while another 10–15% was taken up in the next 8 h. Their findings showed that anion exchange is the main adsorption mechanism for fluoride on Fe3O4/Al2O3 nanoparticles. Activated carbon compounds that were impregnated with nanoparticles had better fluoride removal than regular activated carbon. Zirconium impregnated activated charcoal, made by [20], had 3 to 5 times higher adsorption efficiency than plain activated charcoal. This was because the material had a high positive surface charge, which attracted the negatively charged fluoride ions. The adsorption capacity (q_e) went up from X to Y mg/g as the fluoride concentration increased from 2 to 10 mg/L.

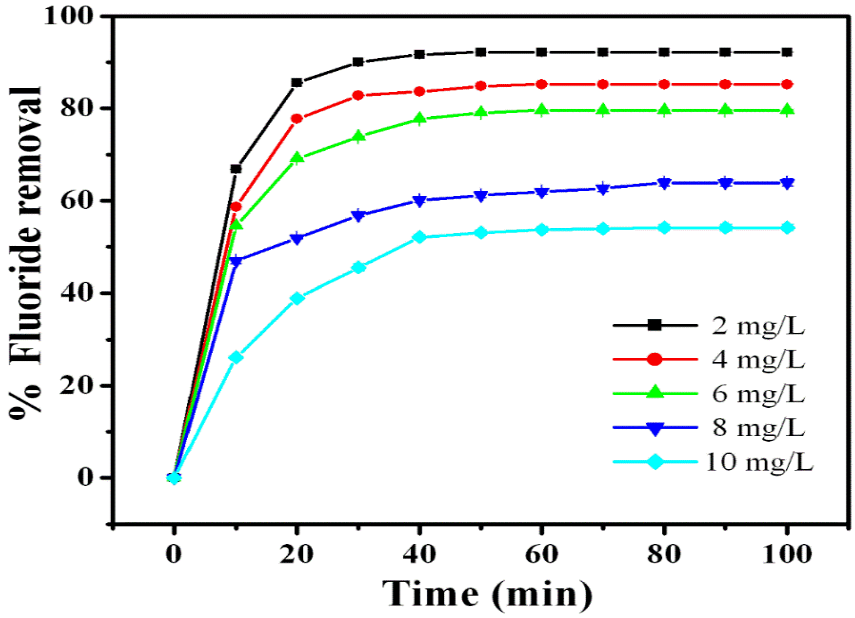

Figure 4. Effect of contact time and initial concentration of F- on the removal of F- from aqueous solutions by NAAC using batch method (Adsorbent dose: 0.2 g/200 mL; pH 7, temperature 30 ± 2).

3.1.2. Adsorption Isotherm

Langmuir and Freundlich adsorption isotherms were used to fit adsorption data at various adsorbate concentrations. Langmuir isotherm is represented as [21]:

$$q_e = (Q_o b C_e)/(1 + bC_e) \quad (2)$$

where C_e is the equilibrium concentration (in mg of adsorbate per liter of solution) and q_e is the amount of adsorbate (in mg per gram of adsorbent) at equilibrium.

The maximum monolayer adsorption capacity is represented by Q_o (in mg of adsorbate per gram of adsorbent), and b is the affinity constant (in liters per mg of adsorbate). A linear version of the Langmuir equation is provided as:

$$C_e/q_e = 1/Q_o b + C_e/Q_o \quad (3)$$

The graphs showing the relationship between q_e and C_e show that the actual results match the expected values from the Langmuir isotherm theory for removing fluoride using the NAAC adsorbent. (Figure 5). In this case, the coefficient of determination (R^2) (Table 1) indicates the ability of the Langmuir equation to adequately describe the experimentally obtained isotherms. The Langmuir constants Q_0 and b were found by looking at the slope and intercept of the graph that shows the Langmuir isotherm in a straight-line form. These values are listed in Table 2. The Freundlich isotherm is a special case of the Langmuir isotherm and is an equation that is used to describe surfaces that are not uniform. It was introduced by [22]. To make the equation easier to work with, we take the logarithm of both sides, which gives the linear form of the Freundlich isotherm:

$$\log q_e = \log K_F + (1/n) \log C_e. \quad (4)$$

where K_F [mg/g (L/mg)n] represents adsorption capacity and n reflects strength of adsorption. Freundlich isotherm did not match the experimental data for F- adsorption, showing average energy adsorption did not decrease as the amount of adsorption increased. Freundlich constants K_F and n are determined from the linear relationship between log q_e and log C_e. (plot not shown). Table 2 shows the K_F and n values. The data clearly show that the adsorption of F- onto the adsorbents does not follow the Freundlich isotherm. The R^2 value for adsorbent materials under the Langmuir isotherm demonstrated greater linearity compared to Freundlich isotherm, suggesting adsorption data align more closely to Langmuir model than with Freundlich model. NAAC showed a Q_0 value of 58.82 mg/g. Its ability to adsorb fluoride was better than most values found in previous studies (see Table 3). Although some recently reported materials exhibit superior adsorption capacity, their complex synthesis process, high cost, and challenges in regeneration hinder broad adoption. In contrast, the current NAAC demonstrates a balance between performance and cost effectiveness.

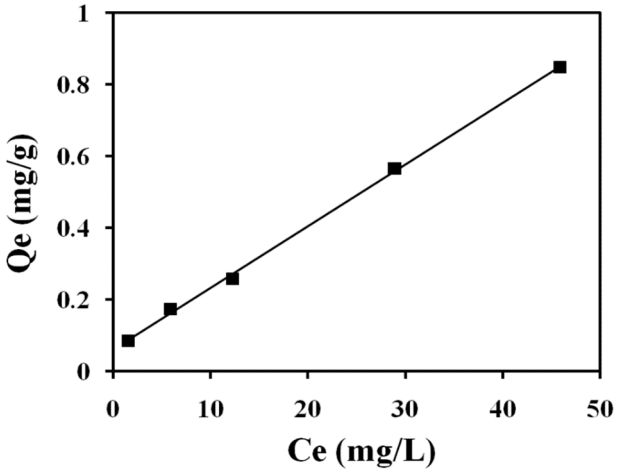

Figure 5. C_e/q_e versus C_e plot used to obtain a linear relationship for Langmuir isotherm.

Table 2. parameters of NAAC for Langmuir and Freundlich isotherm model.

Adsorbent	Langmuir			Freundlich		
	Q_o (mg/g)	b (L/mg)	R^2	K_F (mg/g(L/mg)^n)	n	R^2
NAAC	58.823	0.2833	0.999	17.86	3.125	0.918

Table 3. Maximum F- removal Summary of the capacities by different adsorbents.

S. no	Adsorbents	Adsorption Capacity mg/g	pH	Temp (°C)	Dosage (g/L)	Initial F- (mg/L)	Reference
1	Nanostructured magnesia-impregnated activated carbon	121.1	7.0	25	1.0	10–50	[14]
2	g-C_3N_4-activated carbon composite	92.7	6.5	25	0.5–1.0	10–40	[16]
3	Al_2O_3/CNTs	28.7	7.0	25	1.0	10–30	[23]
4	RS2/$KMnO_4$ carbon	1.438	7.0	30	2.0	5–20	[9]
5	Al-impregnated carbon fibres	17.0	6.0	25	1.0	10–25	[24]
6	Zirconium impregnated carbon	1.83	6.5	25	2.0	5–15	[25]
7	Nano—alumina	14.0	7.0	25	1.0	10–30	[26]
8	Impregnated granular activated carbon of Titanium and Lanthanum oxides	27.8	6.5	25	1.0	10–40	[27]
9	Aluminum Sulfate impregnated Graphene Hydrogel Composites	33.4	7.0	25	0.5	10–50	[28]
10	CGCNT (CTAB grafted carbon Nanotubes)	20.1	7.0	25	1.0	10–25	[28]
11	CeO_2/Al_2O_3 composites	37.0	6.5	25	1.0	10–30	[29]
12	Ca–Al–La composite	29.30	7.0	25	1.0	10–40	[30]
13	Al-doped chitosan–Fe(III) hydrogel	31.16	6.5	25	1.0	10–30	[31]
14	Impregnated magnetic alginate beads of Mg–Al-LDH nanoflake (LDH-n-MABs)	32.4	7.0	25	1.0	10–40	[32]
15	NAAC	58.823	7.0	30 ± 2	1.0 (0.2 g/ 200 mL)	2–10	[32]

Since the fit of the Langmuir isotherm is excellent, there is evidence of homogenous adsorption sites and monolayer formation, meaning that the process of functionalizing the nanoparticles of alumina onto the carbon was successful in creating homogeneous active sites. On the next side, because the Freundlich isotherm doesn't fit well. there is indication of low heterogeneity of the surface, which is a desirable trait when it comes to adsorption in water treatment processes. Adsorption capacity values reported by literature depend greatly on various experimental conditions.

3.1.3. Adsorption Kinetic

Studying adsorption kinetics is of great interest since the rate of the process is one of the essential factors governing its efficiency. The adsorption rate constant was determined using the first-order kinetics model introduced by [33]

$$\text{Log}\,(q_e - q) = \log q_e - (k_1 t/2.303) \quad (5)$$

where q_e and q represent amount for fluoride ions adsorbed (mg/g) at equilibrium and at a certain time t, respectively; and k_1 first-order adsorption rate constant (1/min). Value of q_e and k_1 was found using the regression analysis of a plot showing log (q_e − q) against time t (not shown). The calculated q_e values based on first-order kinetics did not match the actual observed values. Therefore, it can be concluded that the adsorption process did not follow pseudo-first order mechanism. Second-order kinetic model described using following equation

$$t/q = 1/\, k_2 q_e^2 + t/q_e \quad (6)$$

where k_2 are second-order adsorption rate constant [34]. The values of k_2 and q_e were found by analyzing the graph of t/q versus t (Figure 6). The R^2 values show that the fluoride adsorption process fits the second-order model (Table 4). Table 4 compare the first-order and second-order kinetic models for fluoride adsorption using NAAC. The results suggest that the pseudo-second-order equation best explains the adsorption process of fluoride. The mechanism of adsorption was assumed to be chemisorption, since it involves the transfer of electrons from the adsorbent to the adsorbate or the reverse direction. The experimental q_e value was in good agreement with the theoretically calculated value based on the pseudo-second-order kinetics but not with the pseudo-first-order (Table 4).

Kinetic data for pseudo-first and second order have given in Table 4A and Table 4B respectively for easy comparison. Pseudo-first order was find to possess low correlation coefficient values (R^2) together with high difference in experimental q_e and calculated. Pseudo-second order on the other side shows very high correlation coefficient values with the R^2 values ranging from above 0.99. This suggests that chemisorption is the dominant mechanism.

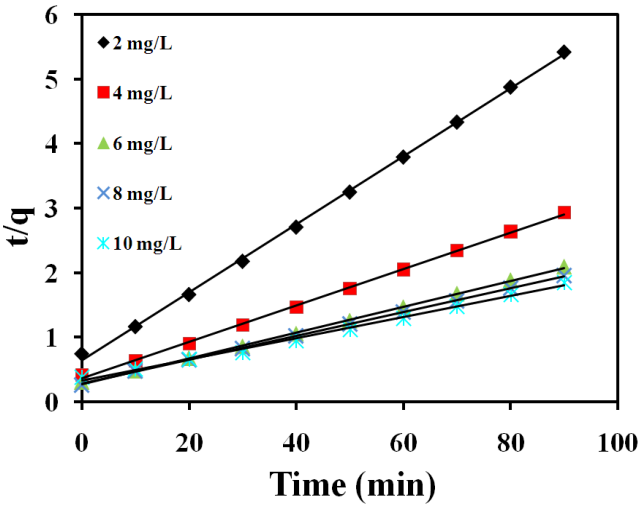

Figure 6. Fluoride adsorption by NAAC for Pseudo second order kinetic model.

Table 4. (**A**) Pseudo first order kinetic model. (**B**) Pseudo-second-order kinetic model.

(A)				
Concentration of Initial F- (mg/L)	**q_e exp (mg/g)**	**q_e cal (mg/g)**	**K_1 min^{-1}**	**R^2**
2	18.43	18.45	0.129	0.685
4	34.10	29.10	0.101	0.710
6	47.70	45.39	0.094	0.744
8	51.10	30.47	0.051	0.763
10	54.10	67.60	0.083	0.860
(B)				
Initial F- Concentration (mg/L)	**q_e (exp) (mg/g)**	**q_e (cal) (mg/g)**	**K_2 (g/mg·min)**	**R^2**
2	18.43	19.23	0.004	0.999
4	34.10	35.71	0.002	0.999
6	47.70	50.00	0.001	0.999
8	51.10	55.56	0.001	0.999
10	54.10	62.50	0.001	0.994

3.1.4. Study in Intra-Particle Diffusion

An observed relationship that works in most adsorption processes follows a graph of uptake versus half-life (called the Weber-Morris model) instead of using contact time. The formula is:

$$q = K_p \times t^{1/2} \quad (7)$$

Here, K_p (in mg g^{-1} $min^{-1/2}$) is the rate constant for particle diffusion. The K_p values were found by looking at the slope of the graph showing q_t versus $t^{1/2}$, as listed in Table 5. The half-life values were used to make the graphs shown in Supplementary Figure S1. The graph for NAAC showing qt versus half-life is in Supplementary Figure S1. It was observed that the plots for both adsorbents were nonlinear which suggested that the adsorption process followed a multi-step mechanism. In this case, the adsorption process consisted of a boundary layer process (initial linear portion) and intra-particle diffusion process (second linear portion). On the other side, the plots showed that intra-particle diffusion is not the only factor limiting how fast fluoride was absorbed by the two adsorbents because the lines did not start at the origin. The intra-particle diffusion model was fitted using the equation ($q_t = K_p \times t^{1/2} + C$), and the results are given in Table 5.

Table 5. fluoride adsorption using NAAC of Intra-particle diffusion parameters.

Initial F- Concentration (mg/L)	**K_p mg g^{-1} $min^{-1/2}$**	**C (mg/g)**	**R^2**
2	1.524	5.21	0.945
4	2.879	9.87	0.952
6	4.105	12.64	0.963
8	4.333	15.12	0.971
10	5.258	18.45	0.978

Intra-particle diffusion constants (K_p and C) were calculated based on the plot between q_t and $t^{1/2}$. The higher fluoride concentration gave rise to higher intercepts (C), which indicated the presence of boundary-layer diffusion effect at high concentrations. It can be observed that the plots do not meet at the origin suggests that the rate is not only controlled by intra-particle diffusion.

3.2. Fluoride Adsorption Using NAAC by Column Mode Process

On an industrial scale, water treatment via adsorption is a continuous process that uses flow-through columns. Thus, it is essential to investigate the removal of toxic metals in flow-through adsorption columns and to examine the potential for using the adsorbents in such systems. Column studies are typically conducted to examine how the material behaves within a dynamic system, and treating water continuously is more cost-effective than using a batch method [35].

3.2.1. Effect of Flow Rate

The way a column-mode treatment works depends a lot on how fast the treatment is done [36]. In this test, we looked at how the speed of the flow affects the removal of fluoride. We used four different flow rates: 2.5, 5.0, 7.5, and 10.0 mL per minute (Figure 7). The setup had a bed volume of 35.32 cm^3 and a fluoride concentration of 6.0 mg/L. At the slowest flow rate of 2.5 mL per minute, 74.4% of the fluoride was removed. The bed became fully used up after 700 mL of eluent was passed through. But when the flow rate was increased from 2.5 to 10 mL per minute, the fluoride removal dropped from 74.4% to 60.5%. This shows that as the flow rate goes up, the amount of fluoride removed goes down. The graph clearly shows that a slower flow rate leads to better fluoride adsorption. On the other hand, higher flow rates lead to poor adsorption due to limited residence time of solute in contact with the column and restricted diffusion of ions into pores of sorbent flow rates at higher [37,38]. The curve indicated that at higher flow rates, the adsorption zone rapidly reached the top and became saturated early. At this stage, the available adsorption sites diminish to negligible or zero levels [39].

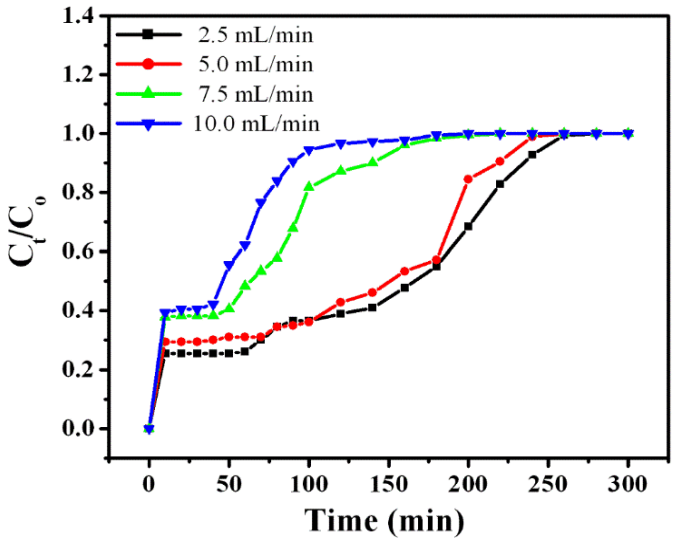

Figure 7. The flow rate affects the removal of fluoride from water using NAAC in a column setup (adsorbate concentration: 6.0 mg/L; bed volume: 35.32 cm^3; pH: 7; temp: 30 ± 2).

3.2.2. Bed Volume Effect

The Bed volume effect of fluoride (F-) removal was examined using the various bed volume of NAAC which include 12.26, 24.53, 49.06 and 73.59 cm^3 with 5 mL/ min flow rate and 6.0 mg/ L adsorbate concentration. As shown in Figure 8, the fluoride increased adsorption with an increase bed volume. From Figure 8 fluoride removal in the treated eluent increased from 46.1% to 82.2% as bed volume increased from 12.26 to 73.59 cm^3 (Figure 8). The increase in adsorption might be because a larger bed volume gives more surface area with active groups that help in capturing the fluoride. It was seen that as the bed volume went up, the breakthrough curve became steeper and the ability to adsorb fluoride also increased [40]. Also, the most fluoride was removed when the bed volume was larger, likely because the adsorbent had more surface area, which means more places for fluoride ions to bind [41,42]. In this study, the best bed volume for removing fluoride from water was 24.53 cm^3 with a flow rate of 5 mL per minute. When more eluent was used, the efficiency of fluoride removal went down because the adsorbent sites became used

up and the movement of fluoride ions wasn't as effective. In addition, there may also be channeling effect and poor effective interaction with the adsorbent in deep beds. Fluoride removal is reduced as a result of early saturation of active site present in adsorbent and also poor mass transfer when using a large eluent volume. Moreover, there might also be channeling effects and poor effective interaction with the adsorbent in deep beds.

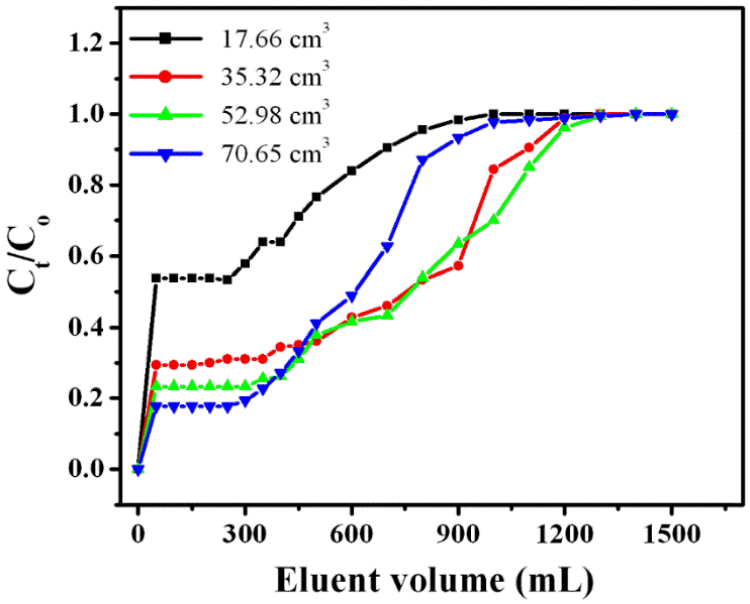

Figure 8. Removal of F- from aqueous solution using NAAC Effect of bed volume on by column mode (adsorbate concentration: 6.0 mg/L; flow rate: 5 mL/min; pH: 7; temp: 30 ± 2).

3.2.3. Initial Adsorbate Concentration Effect

The effect of the starting fluoride level was studied using the best flow speed (5 mL per minute) and bed size (24.53 cm^3). The graphs showed that as the starting concentration went up, the percentage of fluoride removed went down (Figure 9). When the initial concentration was raised from 2 to 10 mg/L, the removal percentage dropped from 95% to 50.3%. A higher initial concentration means more ions are present, which compete for the limited spots where adsorption happens, causing a decrease in how much fluoride can be removed [40]. Additionally, a smaller concentration gradient caused lower ion flux due to the reduced diffusion coefficient. Moreover, increasing in initial conc. of adsorbate resulted a rapid saturation of the adsorbent bed, resulting in shorter breakthrough and exhaustion times for higher initial concentrations [38,43].

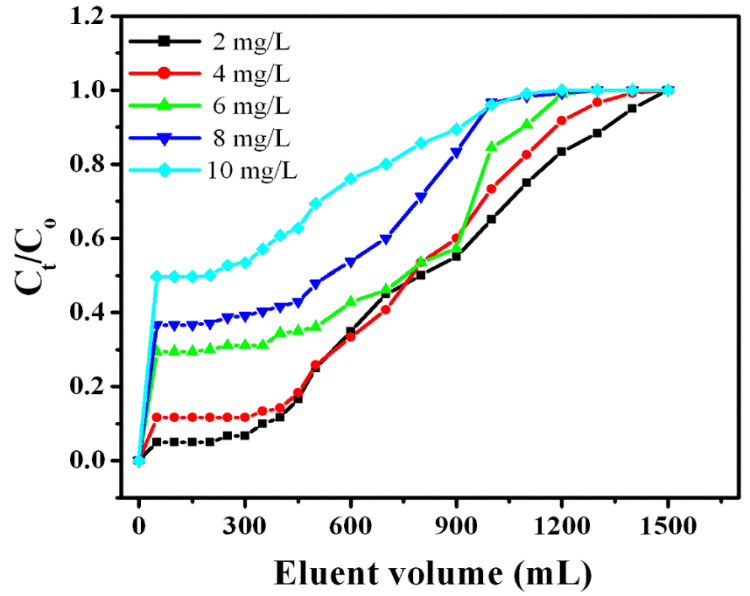

Figure 9. Initial Adsorbate concentration Effect on fluoride removal from aqueous solution by NAAC in a column (flow rate 5 mL/35.32 min bed volume; 7 pH, 30 ± 2 °C temperature).

3.2.4. BDST (Bed-Depth-Service-Time) Model

The BDST model, introduced by [44], gives a simple way to connect many time, t, with different process variables for fixed-bed adsorbents. The BDST curves were created from the data collected, and they can be shown using this equation.

$$C_{ot} = N_0/\mu H - [1/k_a \times \text{In}\ (C_o/C_{t-1}] \quad (8)$$

where t is time it takes for the service to reach breakthrough (in minutes), No is the adsorption capacity (in mg per gram) of the adsorbent bed, C_o is the concentration of the influent (in mg per liter), μ is the linear flow rate (in mg per minute), H is the depth of the bed (in centimeters), K_a is the adsorption rate constant (in liters per minute per mg), and C_t is the concentration of the effluent at time t (in mg per liter). The nonlinear plot for F- removal by the fixed bed according to the BDST model is shown in Supplementary Figure S2. The values of N_0 and K_a for F- adsorption by NAAC shown in Table 6. The adsorption capacity (N_0) of NAAC via column mode was 4.3×10^{-5}, 8.0×10^{-5}, 9.2×10^{-5}, 9.6×10^{-5}, and 7.4×10^{-5} mg/ g for fluoride conc of 2, 4, 6, 8, and 10 mg/ L. Adsorption capacity in bath mode surpasses that in column mode. Therefore, batch sorption was shown to be more effective than column sorption.

Table 6. BDST constants for the removal of F- by NAAC.

Initial F- Concentration mg/L	N_0 (10^{-5}) mg/g	k_a L/mg/min	R^2
2	4.3	5.128	0.98
4	8.0	2.732	0.925
6	9.2	1.706	0.739
8	9.6	1.441	0.833
10	7.4	0.937	0.876

3.3. Mechanism of Adsorption

Mechanism of adsorption of fluoride on iron nanoparticle impregnated activated carbon explained by considering electrostatic attraction by ionic species and the surface functional groups. The highly porous nature and its ability to exchange surface ligands are key factors in adsorbing fluoride ions. Fluoride ions' retention is indirectly justified via kinetic and isotherm modeling, suggesting the process to be chemisorption and monolayer adsorption. Ligand exchange processes involved can be explained by previous findings on alumina-based adsorbents. The adsorption of fluoride on to the NAAC adsorbent used in this study can be related to the ligand exchange mechanism as in the given equation

$$X\text{-}OH + F\text{-} \rightarrow X\text{-}F + OH^- \quad (9)$$

where X is the type of chemical group on the surface of the metal oxide that is attached to the activated carbon. How much substance is taken in depends on how many active hydroxyl groups are on the surface, which is connected to the size of the surface area. All kinds of substances, including protons, fight for the best spots on the nanocomposite material's surface [6]. Evidence for the occurrence of ligand exchange lies in the presence of hydroxyl surface groups in alumina, as demonstrated by EDS measurements that show Al-O composition. Also, the pseudo-second order nature of the kinetics implies chemisorption. However, further confirmation through XPS or TEM-EDS mapping after adsorption would be more convincing. Surface chemical differences and conditions influence the sorption capacity toward nanocomposite. NAAC's strong affinity for fluoride, combined with its high exchange capacity, makes it a suitable choice for removing fluoride. However, not only electrostatic forces are responsible for the observed adsorption of fluoride. The ways fluoride interacts with hydroxyl groups on the nanoparticle surface through surface complexation and ligand-exchange reactions are part of the adsorption process. The homogeneous dispersion of nano-alumina on the surface of carbon is beneficial for the realization of the chemisorption mechanism. Moreover, pseudo-second-order kinetics suggest that chemical reaction is rate-limiting step on this process, which is more significant than physical adsorption. Finally, the strong tendency of fluoride towards the aluminum atom makes the formation of the inner-sphere complexes possible, which leads to the high capacity of adsorption. Modern studies show that the adsorption of fluoride in the hybrid metal oxide-carbon system takes place through physiosorption and chemisorption.

3.4. Desorption Studies

The analysis of desorption capacity will contribute to the estimation of the adsorbent life; therefore, it is essential. The return of desorbed materials and the adsorbent regeneration are also indispensable elements of water

treatment technology [45]. Efforts were undertaken to desorb F- from NAAC using varying concentrations of NaOH (10%). At a 7.5% NaOH concentration, the NAAC adsorbent released the highest amount of fluoride, reaching 55% (Figure 10). The percentage fluoride desorbed maximum and reached saturation after 7.5% NaOH concentration. Fluoride desorption at high pH occurs by replacement of F- group adsorbed onto the adsorbent with OH^- group and CO_3^{2-} when sodium hydroxide used as desorbing agent [46].

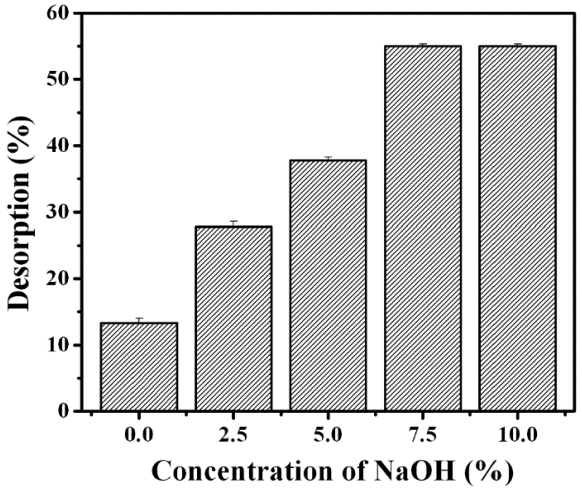

Figure 10. Fluoride desorbed as a percentage at different NaOH concentrations.

4. Conclusions

This study shows that NAAC is good at removing fluoride from water. In batch tests, the adsorption of F- ions onto NAAC depends on factors like contact time, the starting amount of F-, and it works best at a neutral pH and room temperature. The adsorption process matches well with the Langmuir isotherm model and pseudo-second order kinetics. According to the Langmuir model, the maximum adsorption capacity of NAAC is 58.82 mg/g, which means that F- ions form a single layer on the surface of NAAC, and all the sites on the surface have the same attraction for the ions. The nanocomposite shows a strong desorption capacity of 55% when treated with a 7.5% NaOH solution. In column studies, F- adsorption was affected by flow rate, bed volume, and initial adsorbate concentration. However, further studies with continuous multi-cycle reactor designs and scale-up evaluation are needed to completely establish the applicability of the newly developed adsorbent for the industrial sector. based on what you found, what is the main contribution of the study (The NAAC nano adsorbent can be used to create a cheap and effective way to take fluoride ions out of water). This research helps create a good and affordable way to take fluoride out of water by using cheap materials like coir pith and a simple method to make the process work. But still, a thorough cost evaluation and life cycle assessment needs to be done for full validation of its economic viability. Additionally, post-adsorption analyses including TEM-EDS mapping and XPS failed to detect any evidence of fluoride ions binding to the adsorbent surface. This would offer more understanding on the adsorption mechanism. The main goal of future research will be to achieve this. The next phase of our future research will focus on investigating how NAAC behaves in adsorption when competing ions such as sulfate, nitrate, and bicarbonate are present in natural groundwater.

Supplementary Materials

The additional data and information can be downloaded at: https://media.sciltp.com/articles/others/2609241657219392/EPRRI-26010114-SI-FC.pdf.

Author Contributions

S.P.S.: conceptualization, methodology, data curation, writing—original draft preparation; R.S.: visualization, investigation; supervision; validation; reviewing and editing. All authors have read and agreed to the published version of the manuscript.

Funding

The work was funded by the Life Science Research Board (DRDO-LSRB) (Sanction No: LSRB-235/BTB/2011), Govt. of India.

Data Availability Statement

Raw data will be made available on request and approval.

Acknowledgments

Support and help rendered by PSG Management, PSG Institute of Advanced Studies, is acknowledged. The authors are thankful to Anuradha M Ashok, PSG Institute of Advanced Studies, for helping us with HR-TEM analysis.

Conflicts of Interest

The authors declare no conflict of interest.

Use of AI and AI-Assisted Technologies

No AI tools were utilized for this paper.

Abbreviations

NAAC: nano-alumina functionalized carbon composite adsorbent; BDST: Bed-Depth-Service-Time model; XRD: X-ray diffraction; HR-TEM: High Resolution Transmission Electron Microscopy; EDS: Energy Dispersive X-ray Spectroscopy; SAED: Selected Area Electron Diffraction.

References

1. Shaji, E.; Sarath, K.V.; Santosh, M.; et al. Fluoride contamination in groundwater: A global review of the status, processes, challenges, and remedial measures. *Geosci. Front.* **2024**, *15*, 101734.
2. Khan, S.M.; Ravikumar, A. Role of Alkalinity for the Release of Fluoride in the Groundwater of Tiruchengode Taluk, Namakkal District, Tamilnadu, India. *Chem. Sci. Trans.* **2013**, *2*, S302–S308.
3. Singaraja, C.; Chidambaram, S.; Anandhan, P.; et al. Geochemical evaluation of fluoride contamination of groundwater in the Thoothukudi District of Tamilnadu, India. *Appl. Water Sci.* **2014**, *4*, 241–250. https://doi.org/10.1007/s13201-014-0157-y.
4. Duggal, V.; Sharma, S. Fluoride contamination in drinking water and associated health risk assessment in the Malwa Belt of Punjab, India. *Environ. Adv.* **2022**, *8*, 100242. https://doi.org/10.1016/j.envadv.2022.100242.
5. Behera, B.; Kumar, N.; Moharana, M. Assessment of groundwater pollution due to fluoride concentration and water quality in and around Purulia district, West Bengal, India. *J. Chem. Pharm. Res.* **2014**, *6*, 384–392.
6. Suriyaraj, S.P.; Vijayaraghavan, T.; Biji, P.; et al. Adsorption of fluoride from aqueous solution using different phases of microbially synthesized TiO_2 nanoparticles. *J. Environ. Chem. Eng.* **2014**, *2*, 444–454. https://doi.org/10.1016/j.jece.2014.01.013.
7. Suriyaraj, S.P.; Selvakumar, R. Advances in nanomaterial based approaches for enhanced fluoride and nitrate removal from contaminated water. *RSC Adv.* **2016**, *6*, 10565–10583. https://doi.org/10.1039/c5ra24789f.
8. Kumar, R.; Chawla, J. *Carbon-Based Materials for De-Fluoridation of Water: Current Status and Challenges*; IntechOpen: London, UK, 2020. https://doi.org/10.5772/intechopen.90879.
9. Daifullah, A.A.M.; Yakout, S.M.; Elreefy, S.A. Adsorption of fluoride in aqueous solutions using $KMnO_4$-modified activated carbon derived from steam pyrolysis of rice straw. *J. Hazard. Mater.* **2007**, *147*, 633–643. https://doi.org/10.1016/j.jhazmat.2007.01.062.
10. Al-Musawi, T.J.; McKay, G.; Kadhim, A.; et al. Activated carbon prepared from hazelnut shell waste and magnetized by Fe_3O_4 nanoparticles for highly efficient adsorption of fluoride. *Biomass Convers. Biorefin.* **2024**, *14*, 4687–4702.
11. Bakhta, S.; Sadaoui, Z.; Bouazizi, N.; et al. Functional activated carbon: from synthesis to groundwater fluoride removal. *RSC Adv.* **2022**, *12*, 2332–2348. https://doi.org/10.1039/d1ra08209d.
12. Tavallali, H.; Daneshyar, A. Cadmium selenide nanoparticles loaded on activated carbon and its efficient application for removal of fluoride from aqueous solution. *Int. J. ChemTech Res.* **2012**, *4*, 178–181.
13. Guo, S.; Zheng, F.; Xu, J.; et al. Enhanced fluoride removal from drinking water by activated carbon supported Ce-Al oxides: performance and mechanism. *RSC Adv.* **2025**, *15*, 14363–14374. https://doi.org/10.1039/d5ra00397k.
14. Yang, C.; Shen, C.; Zhang, N.; et al. Removing Fluoride from Water by Nanostructured Magnesia-Impregnated Activated Carbon. *Colloids Interfaces* **2025**, *9*, 22. https://doi.org/10.3390/colloids9020022.
15. Sivasankar, V.; Murugesh, S.; Rajkumar, S.; et al. Cerium dispersed in carbon (CeDC) and its adsorption behavior: A first example of tailored adsorbent for fluoride removal from drinking water. *Chem. Eng. J.* **2013**, *214*, 45–54. https://doi.org/10.1016/j.cej.2012.10.023.

16. Pei, S.; Hu, Y.; Huang, Y.; et al. Ultrasonically assisted synthesis of g-C3N4-activated carbon composite for enhanced defluoridation of water. *Alex. Eng. J.* **2024**, *86*, 399–404. https://doi.org/10.1016/j.aej.2023.11.084.
17. Sathishkumar, M.; Binupriya, A.R.; Kavitha, D.; et al. Adsorption potential of maize cob carbon for 2,4-dichlorophenol removal from aqueous solutions: Equilibrium, kinetics and thermodynamics modeling. *Chem. Eng. J.* **2009**, *147*, 265–271. https://doi.org/10.1016/j.cej.2008.07.020.
18. Maliyekkal, S.M.; Sharma, A.K.; Philip, L. Manganese-oxide-coated alumina: A promising sorbent for defluoridation of water. *Water Res.* **2006**, *40*, 3497–3506. https://doi.org/10.1016/j.watres.2006.08.007.
19. Chai, L.; Wang, Y.; Zhao, N.; et al. Sulfate-doped Fe_3O_4/Al_2O_3 nanoparticles as a novel adsorbent for fluoride removal from drinking water. *Water Res.* **2013**, *47*, 4040–4049. https://doi.org/10.1016/j.watres.2013.02.057.
20. Janardhana, C.; Rao, G.N.; Sathish, R.S.; et al. Study on defluoridation of drinking water using zirconium ion impregnated activated charcoals. *Indian J. Chem. Technol.* **2007**, *14*, 350–354.
21. Langmuir, I. The adsorption of gases on plane surfaces of glass, mica and platinum. *J. Am. Chem. Soc.* **1918**, *40*, 1361–1403. https://doi.org/10.1021/ja02242a004.
22. Freundlich, H.M.F. Über die adsorption in lösungen. *Z. Phys. Chem.* **1906**, *57*, 385–470.
23. Li, Y.H.; Wang, S.; Cao, A.; et al. Adsorption of fluoride from water by amorphous alumina supported on carbon nanotubes. *Chem. Phys. Lett.* **2001**, *350*, 412–416. https://doi.org/10.1016/s0009-2614(01)01351-3.
24. Gupta, A.K.; Deva, D.; Sharma, A.; et al. Adsorptive removal of fluoride by micro-nanohierarchal web of activated carbon fibers. *Ind. Eng. Chem. Res.* **2009**, *48*, 9697–9707. https://doi.org/10.1021/ie801688k.
25. Alagumuthu, G.; Rajan, M. Equilibrium and kinetics of adsorption of fluoride onto zirconium impregnated cashew nut shell carbon. *Chem. Eng. J.* **2010**, *158*, 451–457. https://doi.org/10.1016/j.cej.2010.01.017.
26. Kumar, E.; Bhatnagar, A.; Kumar, U.; et al. Defluoridation from aqueous solutions by nano-alumina: Characterization and sorption studies. *J. Hazard. Mater.* **2011**, *186*, 1042–1049. https://doi.org/10.1016/j.jhazmat.2010.11.102.
27. Jing, C.; Cui, J.; Huang, Y.; et al. Fabrication, characterization, and application of a composite adsorbent for simultaneous removal of arsenic and fluoride. *ACS Appl. Mater. Interfaces* **2012**, *4*, 714–720. https://doi.org/10.1021/am2013322.
28. Chen, N.; Zhang, Z.; Feng, C.; et al. Studies on fluoride adsorption of iron-impregnated granular ceramics from aqueous solution. *Mater. Chem. Phys.* **2011**, *125*, 293–298. https://doi.org/10.1016/j.matchemphys.2010.09.037.
29. Zhang, T.; Li, Q.; Mei, Z.; et al. Adsorption of fluoride ions onto non-thermal plasma-modified CeO_2/Al_2O_3 composites. *Desalin. Water Treat.* **2014**, *52*, 3367–3376. https://doi.org/10.1080/19443994.2013.800324.
30. Zhao, X.; Zhang, L.; Xiong, P.; et al. A novel method for synthesis of Co–Al layered double hydroxides and their conversions to mesoporous $CoAl_2O_4$ nanostructures for applications in adsorption removal of fluoride ions. *Microporous Mesoporous Mater.* **2015**, *201*, 91–98. https://doi.org/10.1016/j.micromeso.2014.09.030.
31. Ma, J.; Shen, Y.; Shen, C.; et al. Al-doping chitosan–Fe(III) hydrogel for the removal of fluoride from aqueous solutions. *Chem. Eng. J.* **2014**, *248*, 98–106. https://doi.org/10.1016/j.cej.2014.02.098.
32. Gao, C.; Yu, X.Y.; Luo, T.; et al. Millimeter-sized Mg–Al-LDH nanoflake impregnated magnetic alginate beads (LDH-n-MABs): A novel bio-based sorbent for the removal of fluoride in water. *J. Mater. Chem. A* **2014**, *2*, 2119–2128. https://doi.org/10.1039/c3ta13526h.
33. Lagergren, S. Zur theorie der sogenannten adsorption geloster stoffe. *K. Sven. Vetenskapsakademiens Handl.* **1898**, *24*, 1–39.
34. Ho, Y.S.; McKay, G. Pseudo-second order model for sorption processes. *Process Biochem.* **1999**, *34*, 451–465. https://doi.org/10.1016/s0032-9592(98)00112-5.
35. Kavitha, S.; Selvakumar, R.; Swaminathan, K. Polyvinyl Pyrrolidone K25 Modified Fungal Biomass as Biosorbent for As(V) Removal from Aqueous Solution. *Sep. Sci. Technol.* **2008**, *43*, 3902–3919. https://doi.org/10.1080/01496390802222590.
36. Binupriya, A.R.; Sathishkumar, M.; Dhamodaran, K.; et al. Liquid-phase separation of reactive dye by wood-rotting fungus: A biotechnological approach. *Biotechnol. J.* **2007**, *2*, 1014–1025. https://doi.org/10.1002/biot.200600238.
37. Ko, D.C.K.; Porter, J.F.; McKay, G. Optimised correlations for the fixed-bed adsorption of metal ions on bone char. *Chem. Eng. Sci.* **2000**, *55*, 5819–5829. https://doi.org/10.1016/s0009-2509(00)00416-4.
38. Padmesh, T.V.N.; Vijayaraghavan, K.; Sekaran, G.; et al. Batch and column studies on biosorption of acid dyes on fresh water macro alga Azolla filiculoides. *J. Hazard. Mater.* **2005**, *125*, 121–129. https://doi.org/10.1016/j.jhazmat.2005.05.014.
39. Deepa, K.K.; Sathishkumar, M.; Binupriya, A.R.; et al. Sorption of Cr(VI) from dilute solutions and wastewater by live and pretreated biomass of Aspergillus flavus. *Chemosphere* **2006**, *62*, 833–840. https://doi.org/10.1016/j.chemosphere.2005.04.087.
40. Kamble, S.P.; Deshpande, G.; Barve, P.P.; et al. Adsorption of fluoride from aqueous solution by alumina of alkoxide nature: Batch and continuous operation. *Desalination* **2010**, *264*, 15–23. https://doi.org/10.1016/j.desal.2010.07.001.
41. Vadivelan, V.; Kumar, K.V. Equilibrium, kinetics, mechanism, and process design for the sorption of methylene blue onto rice husk. *J. Colloid Interface Sci.* **2005**, *286*, 90–100. https://doi.org/10.1016/j.jcis.2005.01.007.
42. Mondal, N.K.; Bhaumik, R.; Roy, P.; et al. Investigation on fixed bed column performance of fluoride adsorption by sugarcane charcoal. *J. Environ. Biol.* **2013**, *34*, 1059–1064.

43. Aksu, Z.; Gönen, F. Biosorption of phenol by immobilized activated sludge in a continuous packed bed: prediction of breakthrough curves. *Process Biochem.* **2004**, *39*, 599–613. https://doi.org/10.1016/s0032-9592(03)00132-8.
44. Hutchins, R.A. New method simplifies design of activated carbon systems. *Chem. Eng.* **1973**, *80*, 133–138.
45. Selvakumar, R.; Kavitha, S.; Sathishkumar, M.; et al. Arsenic adsorption by polyvinyl pyrrolidone K25 coated cassava peel carbon from aqueous solution. *J. Hazard. Mater.* **2008**, *153*, 67–74. https://doi.org/10.1016/j.jhazmat.2007.08.020.
46. Veressinina, Y.; Trapido, M.; Ahelik, V.; et al. Catalytic filtration for the improvement of drinking water quality. *Proc. Est. Acad. Sci. Chem.* **2000**, *49*, 168–179. https://doi.org/10.3176/chem.2000.3.04.